Supplementary Table 1. **Synthetic RNA oligonucleotides used in different assays.** This table lists all the RNA oligonucleotides used in this paper. The sequence, length in nucleotides (nt) and the specific identifier used to label the RNA in the experimental descriptions are provided. All RNAs were chemically synthesized by Biomers.

	Length [nt]	**Identifier**	**Sequence**		
5′ RNA	20	L 5′ (1-20)	5′ HO-	ACACAGAGACGCCCAGAUGA	-OH 3′
	21	S_{9A} 5′ (1-21)	5′ HO-	ACACAAAGAACCCCCUUCAUU	-OH 3′
3′ RNA	20	L 3′ (1-20)	3′ HO-	UGUGUUUCUGGCGGGUCUAG	-OH 5′
	26	L 3′-6A (1-26)	3′ HO-	UGUGUUUCUGGCGGGUCUAGAAAAAA	-OH 5′
	21	S_{9U} (1-21)	3′ HO-	UGUGUUUCUUGGGGGUUUUUU	-OH 5′
Primer	2	Primer AC	5′ HO-	AC	-OH 3′
	17	Primer B-OH	5′ HO-	AAACGCAACAACAACA	-OH 3′

Supplementary Table 2. **Cryo-EM data collection, processing, refinement, and validation statistics.** This table provides the parameters and statistics for the data collection, processing, refinement, and structure validation of the cryo-EM structures. Refinement statistics were generated using the Phenix package.

	5′ HOOK	**EARLY ELONGATION**	**EARLY ELONGATION ENDO**	**LATE ELONGATION**	**RESTING**
PDB Code	8AS6	8AS7	8ASB	8ASD	8ASG
EMBD Code	EMD-15607	EMD-15608	EMD-15610	EMD-15614	EMD-15615
Data collection and processing					
Microscope	Titan Krios G3	Titan Krios G3			Titan Krios G3
Voltage (kV)	300	300			300
Camera	Gatan K3 BioQuantum	Gatan K3 BioQuantum			Gatan K3 BioQuantum
Magnification	105,000	105,000			105,000
Nominal negative defocus range (μm)	0.8 – 2.5	0.8 – 2.5			0.8 – 2.5
Exposure time (s)	2.5	2.5			2.5
Electron exposure (e-1/Å^2)	55	53			55
Frames collected (no.)	50	50			50
Frames processed (no.)	50	50			50
Pixel size (Å)	0.85	0.85			0.85
Micrographs (no.)	3,178	3,547			2,985
Total particle images	1,648k	2,651k			278k
Refinement					
Final particle subset (no.)	60k	89k	16k	60k	37k
Map resolution (Å), 0.143 FSC	3.4	2.6	3.6	2.6	3.2
Map sharpening *B* factor (Å^2)	-93	-40	DeepEMhancer	-37	Local Filter
Map vs. model cross-correlation CC-MASK	0.83	0.82	0.73	0.84	0.82
Model composition					
Non-hydrogen atoms	12784	13431	14487	15533	12689
Protein residues	1566	1575	1715	1826	1544
Nucleotide residues	14	37	38	44	17
Waters	0	10	0	32	0

Other	N/A	2 Mg, 1 nhUTP, 1 HEPES	1 Mg, 1 nhUTP	3 Mg, 1 nhUTP	1 Mg
Mean B factors (Å)					
Protein	66.16	42.93	78.81	41.97	68.49
Nucleotide	73.61	62.80	86.61	41.04	102.60
Ligand	N/A	47.44	71.60	27.38	47.52
Water	N/A	28.40	N/A	28.35	N/A
R.m.s. deviations					
Bond lengths (Å)	0.004	0.003	0.003	0.004	0.003
Bond angles (°)	0.709	0.619	0.682	0.653	0.736
Validation					
MolProbity score	1.70	1.47	1.73	1.42	1.70
All-atom clashscore	4.32	5.32	6.72	3.96	6.56
Poor rotamers (%)	0.00	0.29	0.07	0.06	0.29
Ramachandran plot					
Favoured (%)	91.95	96.87	94.74	96.37	95.15
Allowed (%)	8.05	3.13	5.26	3.63	4.85
Outliers %)	0.00	0.00	0.00	0.00	0.00

Supplementary Table 3. **Raw data from RVFV mini replicon assays.** For each mutant, the calculated Ren-Luc activity (as a % compared to the WT) from 3 biological replicates (as indicated in the table), the calculated average and standard deviation is provided.

RVFV Residue(s)	Replicate 1	Replicate 2	Replicate 3	Average	Standard Deviation
Set 1 – Hook Interacting Residues					
E312A	101,18	102,42	123,95	109,18	10,45
D313A	50,48	113,73	100,23	88,15	27,20
Q326A	97,83	115,05	93,20	102,02	9,40
G418V	0,02	0,01	0,01	0,01	0,01
K422A	38,34	48,68	45,85	44,29	4,36
R434A	51,86	78,88	74,13	68,29	11,78
K533A	86,89	130,18	151,11	122,73	26,74
F561A	2,82	7,75	8,33	6,30	2,47
K602A	74,50	96,79	121,88	97,72	19,35
K661A	0,12	0,08	0,41	0,20	0,15
R700A	0,02	0,01	0,01	0,01	0,01
V698G	30,42	89,70	79,89	66,67	25,94
E769A	102,07	129,69	171,22	134,33	28,42
S771A	103,28	184,97	173,16	153,80	36,05
I1041G	4,38	5,65	8,13	6,05	1,56
H1045A	3,50	3,13	2,87	3,17	0,26
V1055G	42,86	82,81	48,38	58,02	17,68
F1059A	0,02	0,04	0,01	0,02	0,01
S437A/K438A	22,75	38,12	27,38	29,42	6,44
D1049A/R1051A	35,39	42,69	27,07	35,05	6,38
Set 2 – 3′ Secondary Binding Site					
R396A	10,17	14,25	10,17	11,53	1,92
R401A	0,03	0,03	0,07	0,04	0,02
E523A	0,02	0,01	0,01	0,01	0,01
K540A	0,01	0,01	0,02	0,01	0,00
V596A	36,44	32,44	24,65	31,18	4,89
K1420A	28,30	52,39	45,12	41,94	10,09
V1426G	0,07	0,01	0,03	0,04	0,02
K1449A	6,54	15,53	20,06	14,04	5,62
D376A_D377A	4,24	9,62	7,83	7,23	2,24
K529A_Q530A	5,89	7,56	4,17	5,87	1,39
Set 3 – Priming Loop-like/Active Site Residues					

R1204A	0,04	0,08	0,03	0,05	0,02
R1204K	39,40	46,17	33,70	39,76	5,10
H1090A	0,03	0,03	0,01	0,02	0,01
Y1091A	0,95	0,21	2,90	1,35	1,14

SFTSV – 5’ HOOK

3178 Movie frames
WARP picking: 1648k particles
2D classification: 1648k particles

3D classification in 10 classes (514k particles – Bin 4)

Other low resolution classes

Particle extraction (102k particles – Bin 1)

5’ HOOK

3D Refinement
(102k particles), 3.9 Å

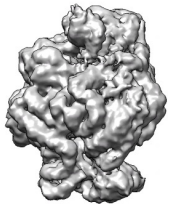

Aberration corrections, Bayesian polishing,
3D Refinement
(60k particles), 3.4 Å

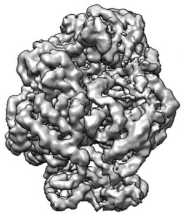

Supplementary Figure 1. **Cryo-EM data processing workflow for the SFTSV L 5′ HOOK dataset.** After micrograph pre-processing and BoxNet particle picking in Warp [40], particles were extracted using a binning factor of 4 in RELION [37,38] for 2D classification. 2D classes that had visible protein secondary structure were selected for subsequent 3D classification (514k particles). The particles were classified into 10 classes for 3D classification with angular assignment. Incomplete, low resolution or classes containing damaged particles were excluded from further data analyses. Particles from a single class, denoted 5′ HOOK, were re-extracted with the original pixel size value and refined before further 3D classification without angular assignment. The final particle subset was CTF refined, Bayesian polished and post-processed in RELION 3.1/4.0 [37,38].

SFTSV – 5’ HOOK

A

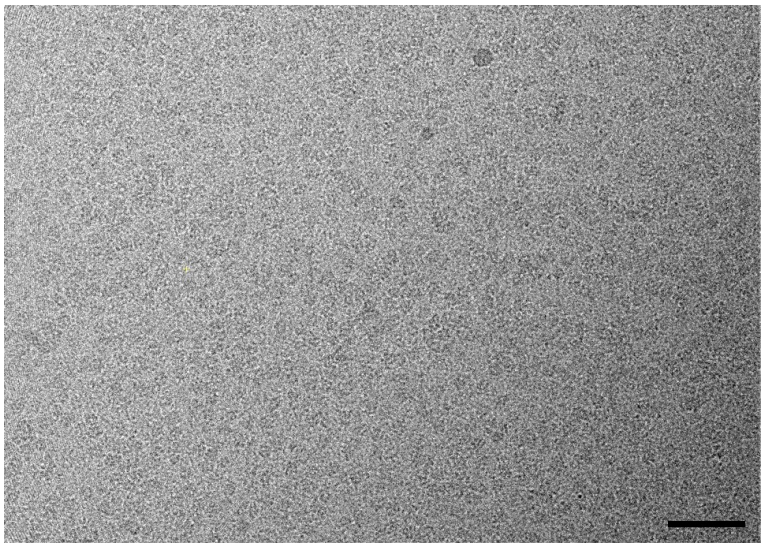

B

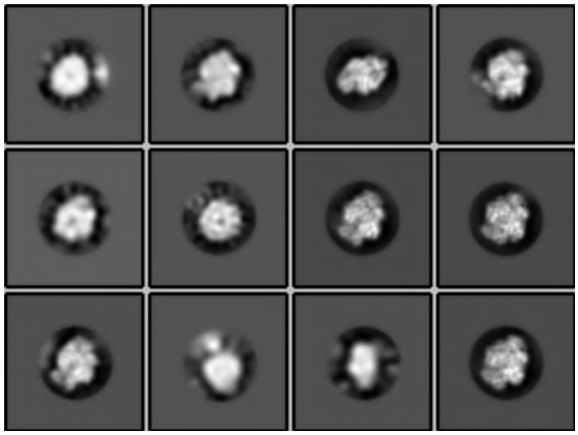

C

5’ HOOK

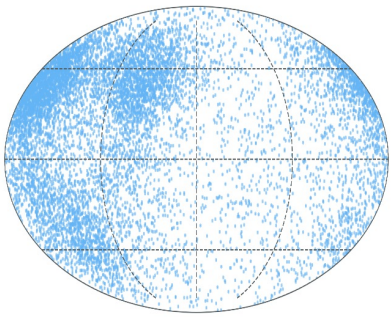

D

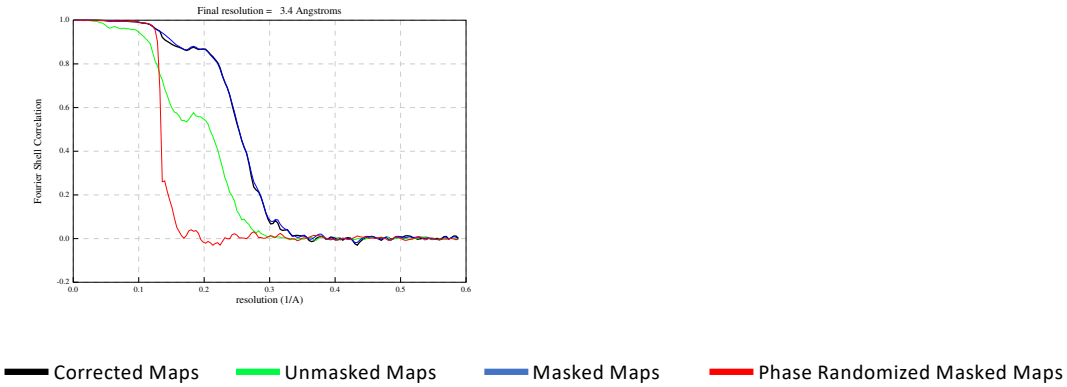

E

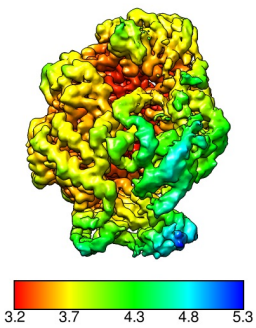

Supplementary Figure 2. **Cryo-EM of SFTSV L protein bound to the 5′ RNA (5′ HOOK).** (A) A representative micrograph of SFTSV L protein in free standing ice after MotionCor2 [39] correction at defocus of ~2.0 µm. (B) Most populated 2D class averages of the of SFTSV L protein bound to the 5′ hook primer (see Materials and Methods). (C). Angular distribution for all of the particles refined visualized on a globe-like plane. (D) Fourier shell correlation (FSC) curves for the final refined class. The plot of the FSC between two independently refined half maps shows the overall resolution as indicated by the gold standard criteria of the FSC cut-off at 0.143. (E) Surface representation of the local resolution distribution of the final class after refinement. Maps are coloured according to the local resolution calculated within the RELION software package [37,38] and displayed in Chimera [42]. Resolution is as indicated in the colour bar.

SFTSV – ELONGATION

3547 Movie frames
WARP picking: 2651k particles
2D classification: 2651k particles

3D classification in 12 classes (2651k particles – Bin 4)

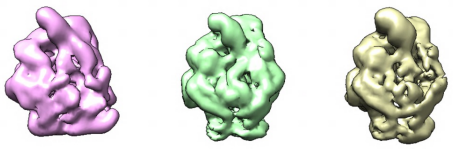

Other low resolution classes

3D classification in 10 classes (1107k particles – Bin 1)

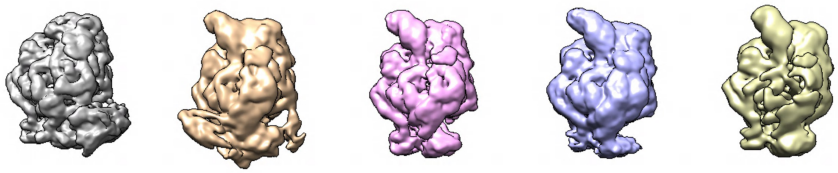

Other low resolution classes

LATE-ELONGATION

3D Refinement
(132k particles), 3.0 Å

Highest resolution class from
3D Classification
without image alignment

Aberration corrections
Bayesian polishing
3D Refinement
(60k particles), 2.6 Å

EARLY-ELONGATION-ENDO

3D Refinement
(88k particles), 3.3 Å

Highest resolution class from
masked 3D Classification
without image alignment

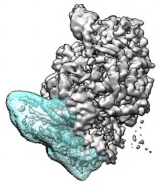

Aberration corrections
Bayesian polishing
3D Refinement (16k particles), 3.6 Å

EARLY-ELONGATION

3D Refinement
(470k particles), 3.0 Å

Highest resolution class from
3D Classification
without image alignment

Aberration corrections
Bayesian polishing
SIDESPLITTER 3D Refinement
(89k particles), 2.6 Å

Supplementary Figure 3. **Cryo-EM data processing workflow for the SFTSV L elongation dataset.** After micrograph pre-processing and BoxNet particle picking in Warp [40], particles were extracted using a binning factor of 4 in RELION [37,38] for 2D classification. 2D classes were used for initial check but not to filter out particles so all picked particles went into 3D classification (2651k particles). The particles were classified into 12 classes for 3D classification with angular assignment. Incomplete, low resolution or classes containing damaged particles were excluded from further data analyses. The remaining particles were then re-extracted with original pixel size for further 3D classification using 10 classes. Among these, 3 classes with visible protein secondary structure were pooled as ‘‘EARLY ELONGATION’’. These had density where we expect binding of an RNA duplex and were globally 3D refined. In parallel, 2 additional classes, each with distinct features, were refined independently. The so-called ‘‘EARLY ELONGATION ENDO’’ had a poor density for the endonuclease domain which was then masked for a subsequent 3D classification without image alignment. Afterwards, the highest resolution class showing a clear density for the endonuclease after refinement. The ‘‘LATE ELONGATION’’ class, was 3D refined before being further 3D classified without image alignment. The highest resolution class was then selected for further refinement. Final particle subsets were CTF refined, Bayesian polished and post-processed in RELION 3.1/4.0 [37,38].

SFTSV – ELONGATION

A

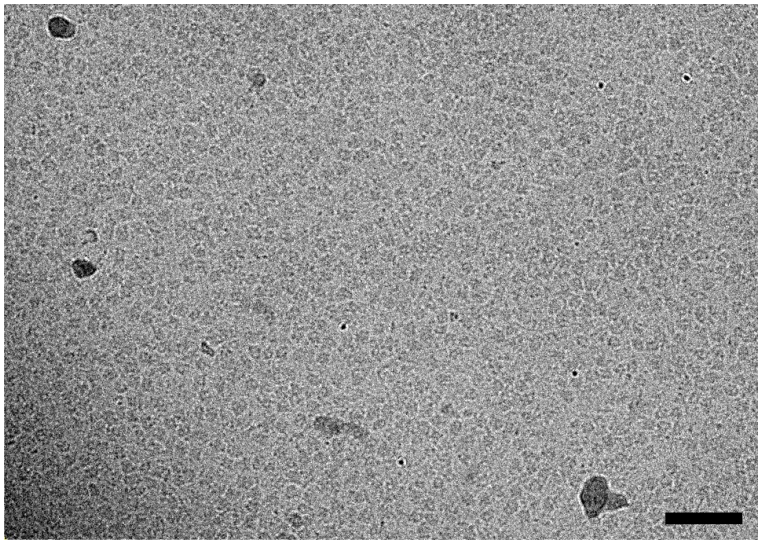

B

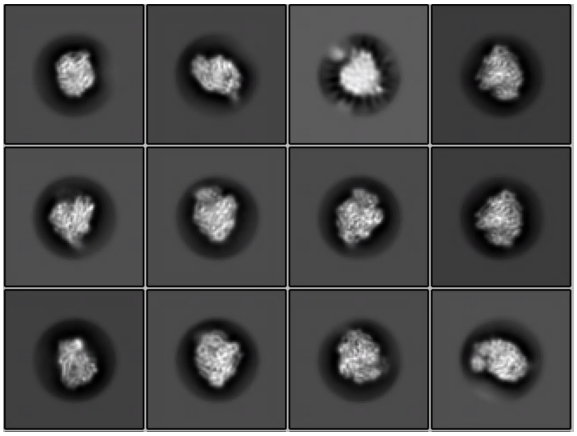

C

LATE-ELONGATION | **EARLY-ELONGATION-ENDO** | **EARLY-ELONGATION**

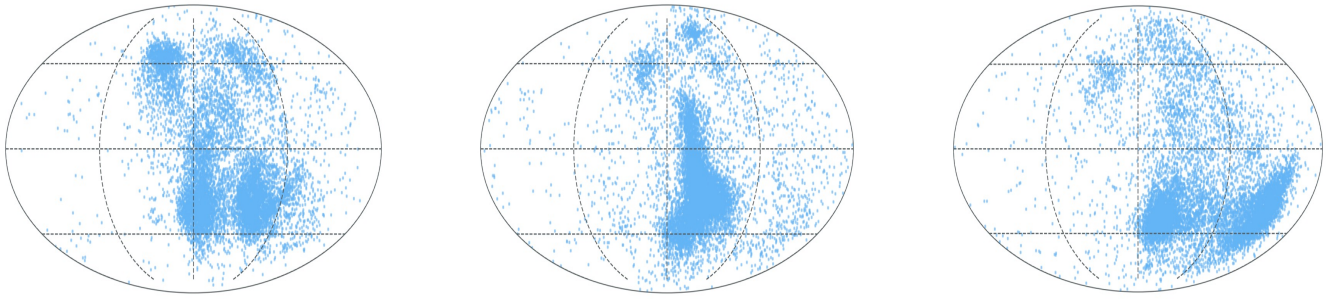

D

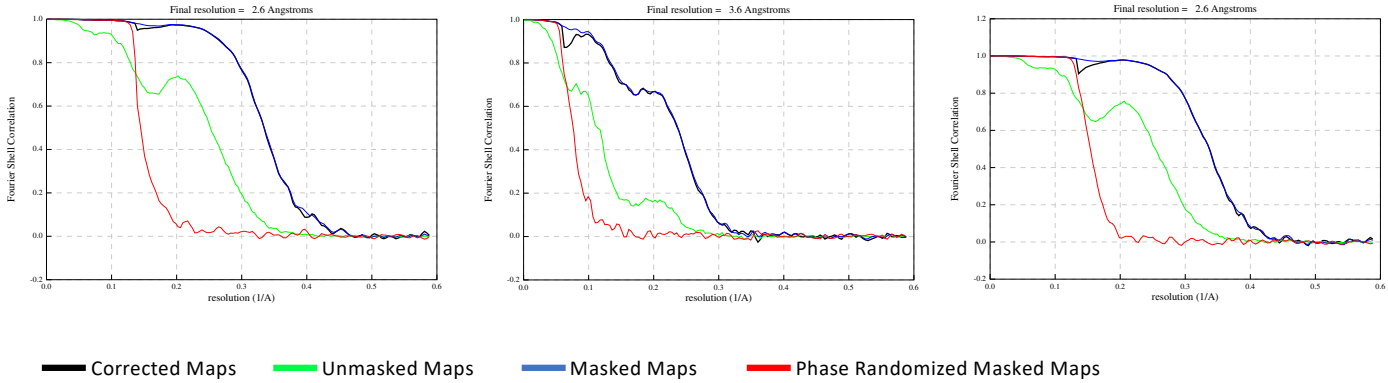

E

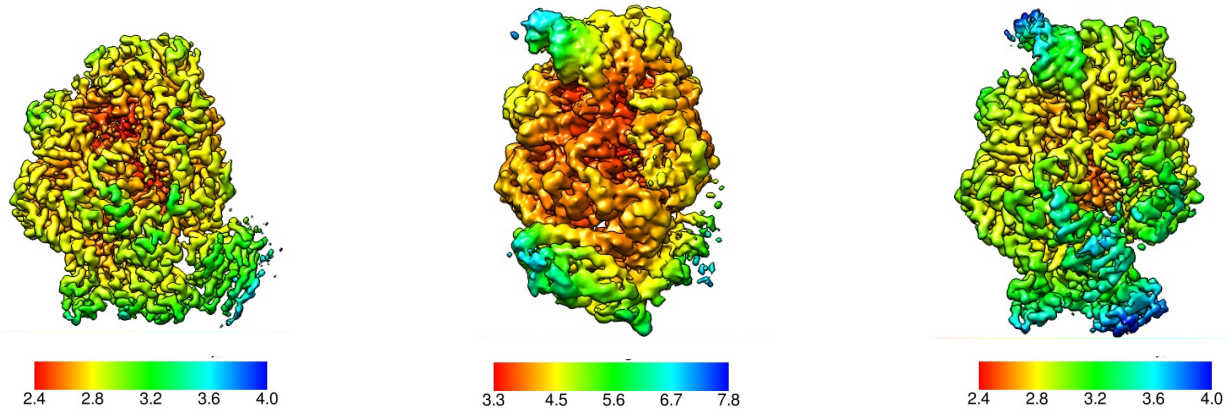

Supplementary Figure 4. **Cryo-EM of the SFTSV L protein elongation reaction.** (A) A representative micrograph of SFTSV L protein in free standing ice after MotionCor2 [39] correction at defocus of ~2.0 µm. (B) A selection of the most populated 2D class averages of the of SFTSV L protein stalled with nhUTP (see Materials and Methods). (C) Angular distribution for all of the particles contributing to the different refined classes visualized on a globe-like plane. (D) Fourier shell correlation (FSC) curves for each final refined class. The plot of the FSC between two independently refined half maps shows the overall resolution as indicated by the gold standard criteria of the FSC cut-off at 0.143. (E) Surface representation of the local resolution distribution of each final class after refinement. Maps are coloured according to the local resolution calculated within the RELION software package [37,38] and displayed in Chimera [42]. Resolution is as indicated in the colour bar.

SFTSV – RESTING

4385 Movie frames
WARP picking: 278k particles
2D classification: 278k particles

↓

3D classification in 8 classes (278k particles – Bin 4)

Other low resolution classes

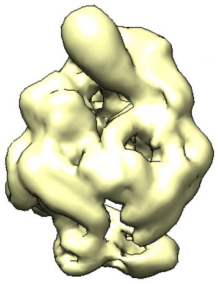

↓

Particle extraction (74k particles – Bin 1)

↓

RESTING

3D Refinement
(74k particles), 3.4 Å

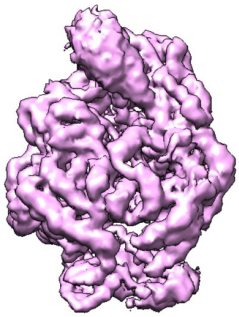

↓

3D Classification without image alignment
Highest resolution class

↓

Aberration corrections, Bayesian polishing,
cryoSPARC non-uniform Refinement
(37k particles), 3.2 Å

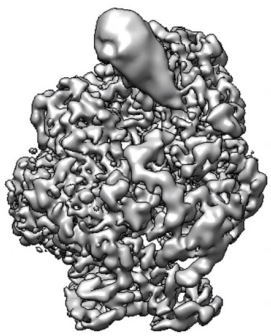

Supplementary Figure 5. **Cryo-EM data processing workflow for the SFTSV L RESTING dataset.** After micrograph pre-processing and BoxNet particle picking in Warp [40], particles were extracted using a binning factor of 4 in RELION [37,38] for 2D classification. 2D classes were used for initial check but not to filter out particles so all picked particles went into 3D classification (278k particles). The particles were classified into 8 classes for 3D classification with angular assignment. Incomplete, low resolution or classes containing damaged particles were excluded from further data analyses. A single class, "RESTING", showed secondary structure features which was selected for further processing. Particles were re-extracted with the original pixel size value and refined before a subsequent 3D classification without image alignment with the highest resolution class selected for further 3D refinement. Final particle subset was CTF refined and Bayesian polished in RELION 3.1/4.0 [37,38] prior to being subjected to non-uniform refinement and post-processed in cryoSPARC [43,44].

SFTSV – RESTING

A

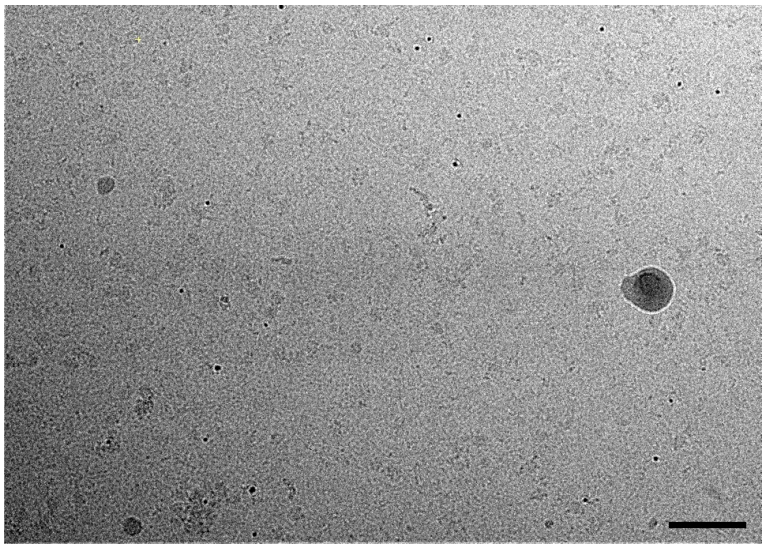

B

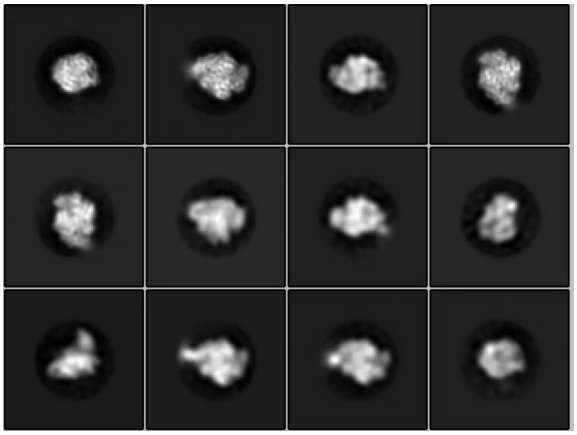

C

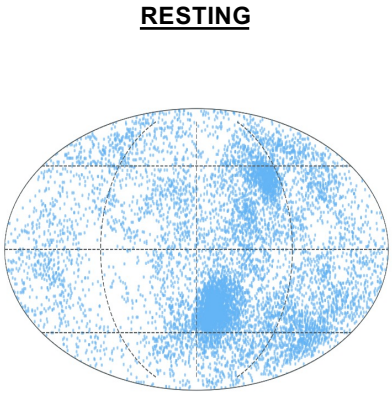

D

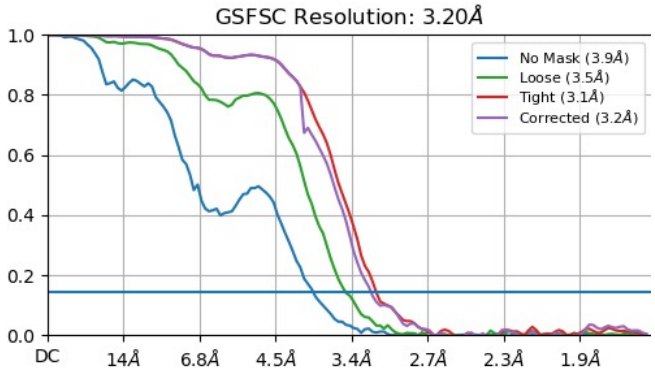

E

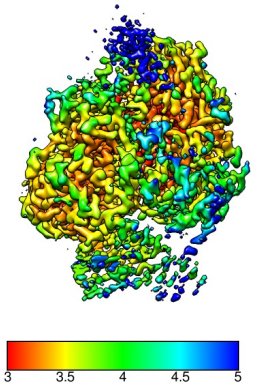

Supplementary Figure 6. **Cryo-EM of the SFTSV L RESTING dataset.** (A) A representative micrograph of SFTSV L protein in free standing ice after MotionCor2 [39] correction at defocus of ~2.0 µm. (B) A selection of the most populated 2D class averages of the SFTSV L protein bound to AC primer (see Materials and Methods). (C) Angular distribution for all of the particles refined visualized on a globe-like plane. (D) Fourier shell correlation (FSC) curves for the final refined class. The plot of the FSC between two independently refined half maps shows the overall resolution as indicated by the gold standard criteria of the FSC cut-off at 0.143. (E) Surface representation of the local resolution distribution of each final class after refinement. Maps are coloured according to the local resolution calculated within the RELION software package [37,38] and displayed in Chimera [42]. Resolution is as indicated in the colour bar.

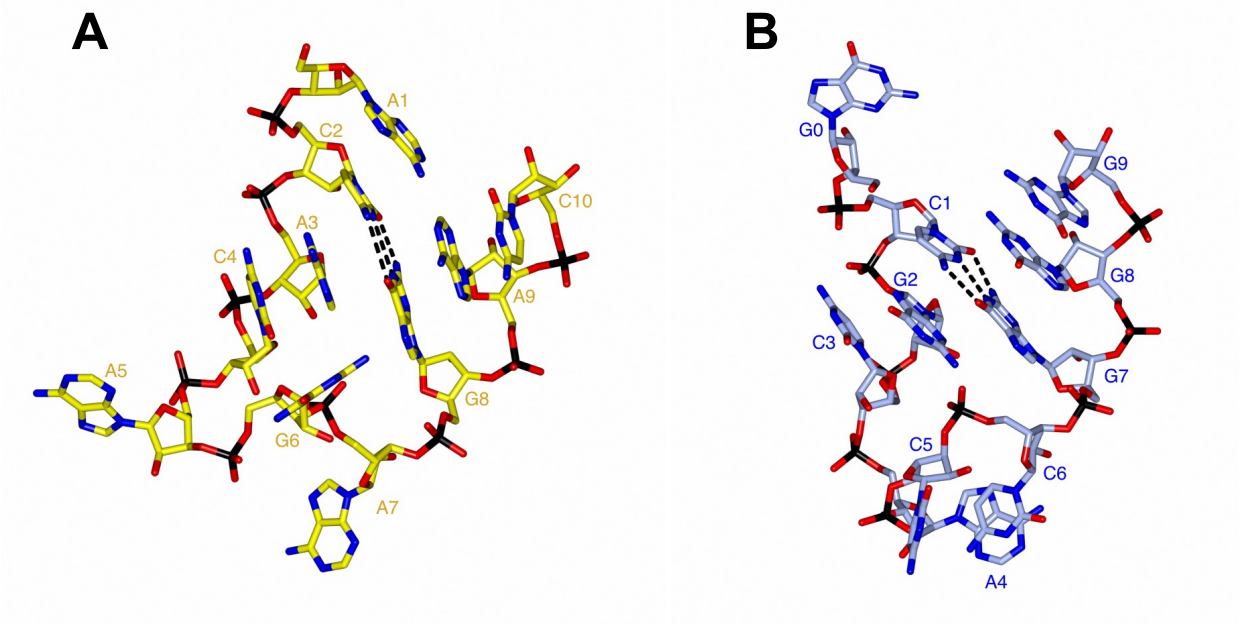

SFTSV

LASV
(PDB: 7OJN)

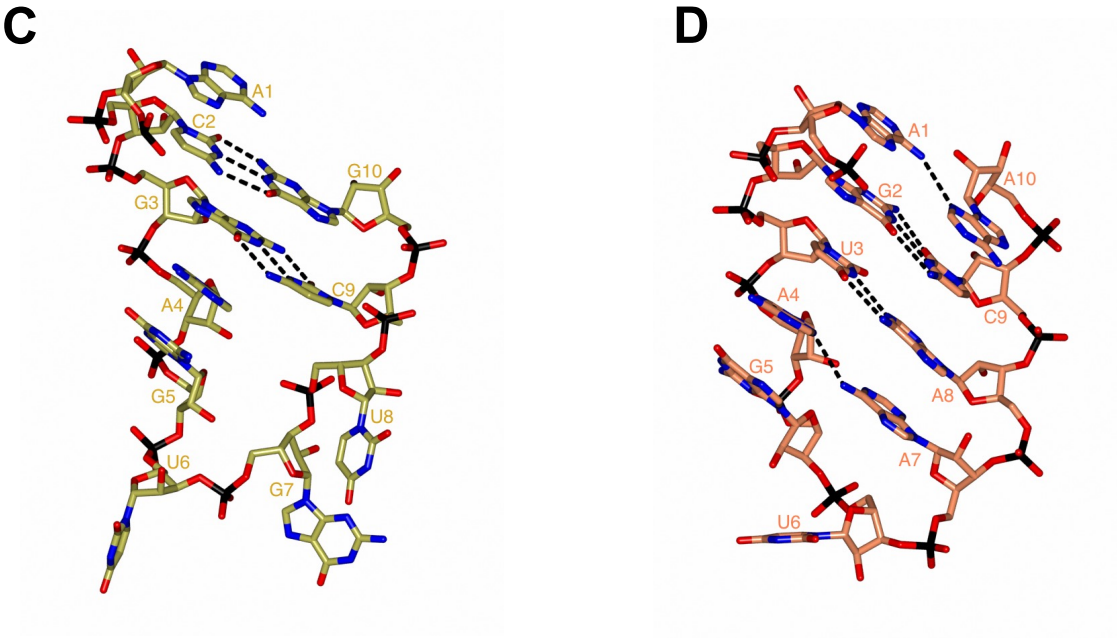

LACV
(PDB: 7ORN)

Influenza virus
(PDB: 6T0V)

Supplementary Figure 7. **Comparison of known 5′ RNA hook structures for sNSVs.** The 5′ RNA hook structures of SFTSV (A), LASV (B, nts 1-10 from PDB: 7OJN), LACV (C, nts 1-10 from PDB: 7ORN), and Influenza virus (D, nts 1-10 from PDB: 6T0V) are shown as sticks. Individual bases are labelled from the 5′ end and base-pairing interactions are shown as dotted lines.

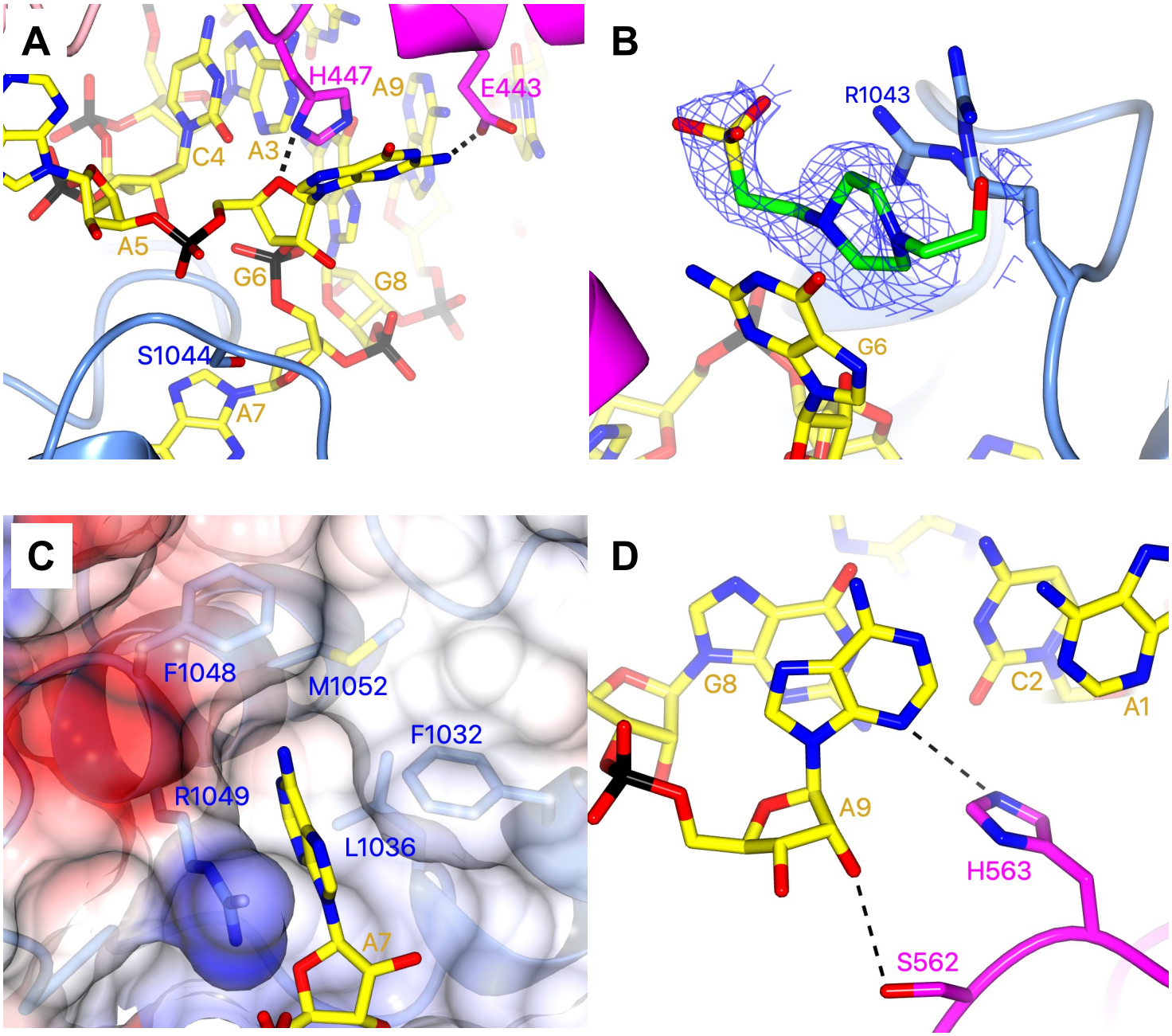
A
H447
A9
E443
C4
A3
A5
G6
G8
S1044
A7
B
R1043
G6
C
F1048
M1052
F1032
R1049
L1036
A7
D
G8
C2
A1
A9
H563
S562

Supplementary Figure 8. **Coordination of the SFTSV 5′ RNA hook.** (A) Coordination of G6 by S1044 and H447. (B) Stacking of a single HEPES molecule between the G6 base and the R1043 sidechain. The shown map is clipped to the HEPES monomer and contoured at 2σ. (C) Coordination of the A7 base which sits in a relatively tight pocket delineated by several hydrophobic residues including F1032, L1036, and F1048. Surface electrostatics for these residues is also shown and coloured according to standard practice. (D) Coordination of the A9 base which is shown interacting with S562 and H563. For clarity, the next bases in the 5′ RNA are not shown. In each panel, direct interactions are shown as dotted lines.

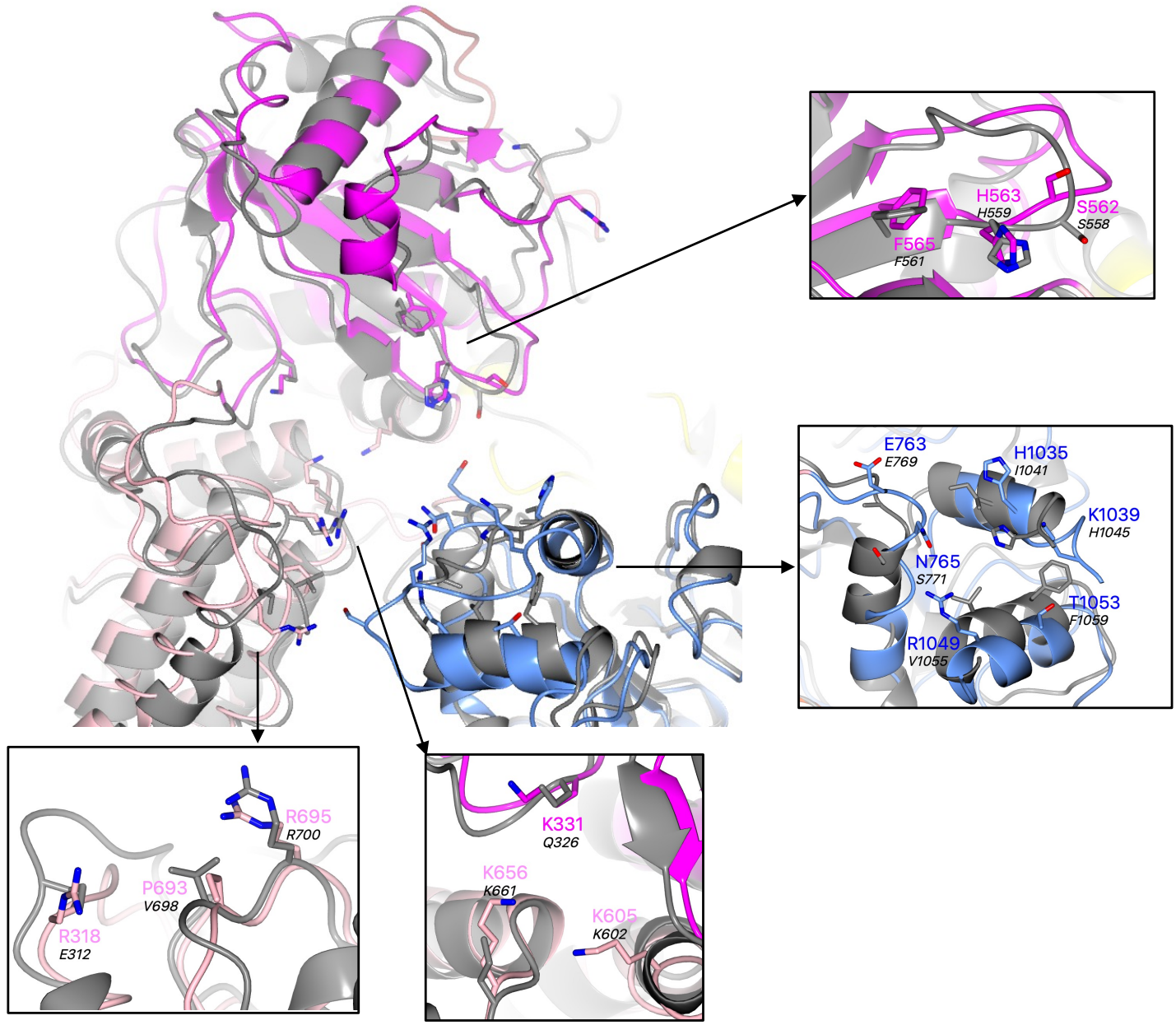


```
      310                                          340   420                                          455
SFTSV DLLAGLHAR-SNKQTSLNRGTVKLPPWLPKPS  …   RQEFSLQGVEGKKWKRMAANQKKEKESHETLSPFLD
RVFV  RALNQYRAEDNLRDLNDHKSTIQLPPWLSYHD  …   SVYIAALGVNGKKHKADTLVQQMRDRSKQPFSPDHD

      456  460  520                                                    570  600        609
SFTSV VEDIG … WVSCLAQELASALKQHCRAGEFIIKKLKFWPIYVIIKPTKSSSHIFYSLGI …  SLKTCKLTNL
RVFV  VDHIS … MVSLIGAELSASVKQHVKPNYFVIKRLLGSGIFLLIKPTSSKSHIFVSFAI …  SYKLSKLTNL

      610                                                            660  690        699
SFTSV VNLPCTMLNSIAFWREKLGVAPWLVRKPCSELR--------EQVGLTFLISLEDKSKTE …  LDGPLRTKLQ
RVFV  CKCVSLMESSFSFWAEAFGIPSWNFVGDLFRSSDSAAMDASYMGKLSLLTLLEDKAATE …  FPKVLRSELQ

      760         770  1030                                  1060
SFTSV ESTELNALGEM  …  LRFLAHLSSKSESRSSDPFREAMTDAFHGNR
RVFV  EETEPSSLSGM  …  LNYLKILDGHRELDIRDDFVMDLFKAYHGEA
```

Supplementary Figure 9. **Structural superposition of the RVFV L protein onto the SFTSV L protein (hook binding site focus).** The SFTSV L protein (5′ HOOK) is shown with the RVFV L protein (PDB: 7EEI, backbone coloured grey) superposed by SSM in CCP4mg [51]. Sidechains of key amino acids mutated in the cell-based mini-replicon are shown individually with close-up views. Several RVFV L protein amino acid sidechains appear truncated, this is because they were truncated in the 7EEI structure by the depositing authors. Residues from the SFTSV L protein are labelled and coloured according to the assigned domain (pink for the PA-C like-domain, blue for the fingers, and magenta for the vRBL) with the corresponding RVFV L protein residue labelled in black. For clarity, not all residues mutated in the cell-based mini-replicon are shown but 15 of the 23 in total are shown. A multiple-alignment diagram showing the SFTSV (UniProtKB: F1BV96) and RVFV (UniProtKB: A2SZS3) L protein chains generated using Clustal Omega [77] is also provided. Residues mutated in the RVFV mini-replicon system are in bold with single mutants coloured red and double-mutants coloured blue.

[77] Sievers, F., Wilm, A., Dineen, D., Gibson, T.J., Karplus, K., Li, W., Lopez, R., McWilliam, H., Remmert, M., Soding, J. et al. (2011) Fast, scalable generation of high-quality protein multiple sequence alignments using Clustal Omega. Mol Syst Biol, 7, 539.

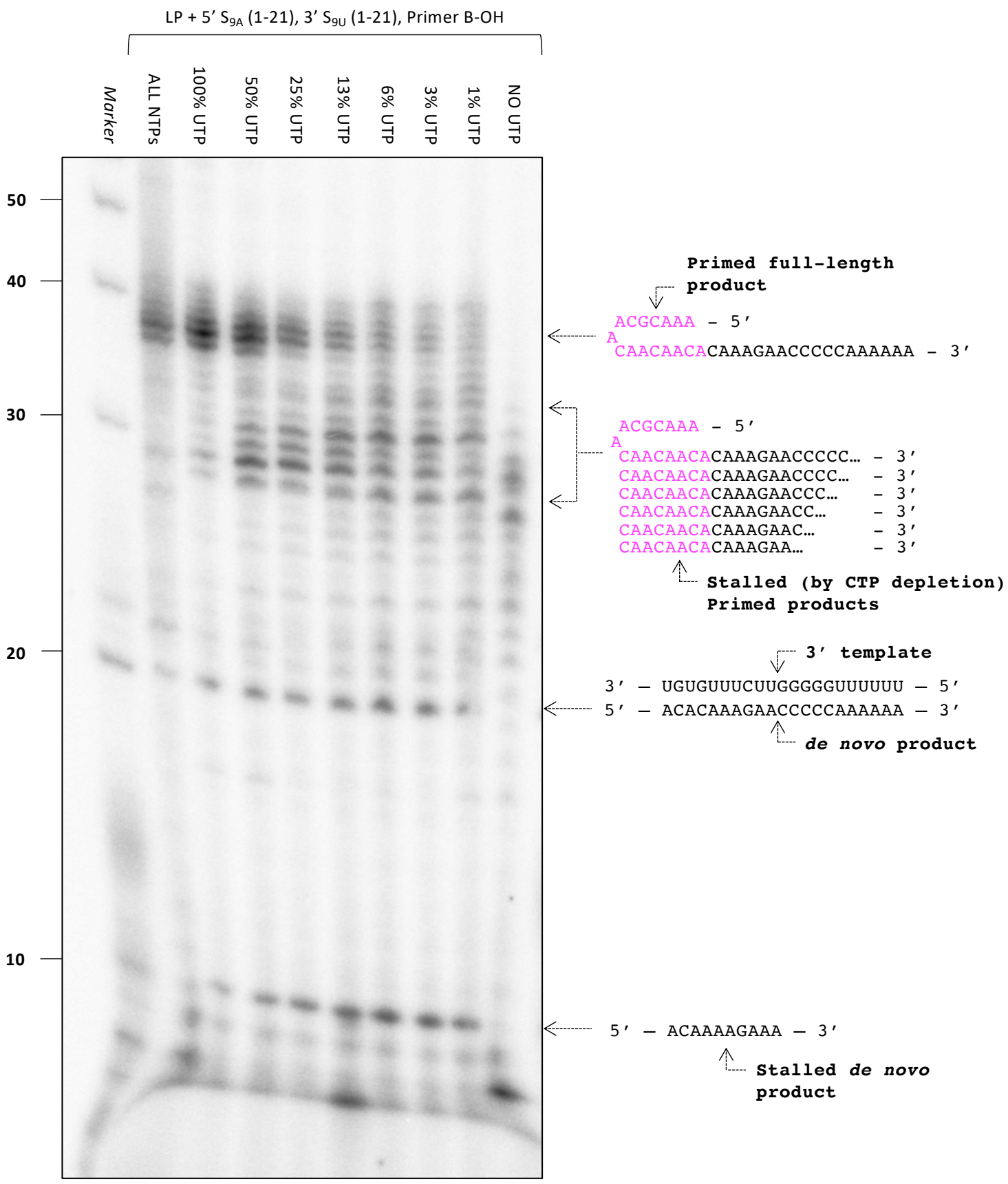
LP + 5′ S9A (1-21), 3′ S9U (1-21), Primer B-OH
Marker
ALL NTPs
100% UTP
50% UTP
25% UTP
13% UTP
6% UTP
3% UTP
1% UTP
NO UTP
50
40
30
20
10
Primed full-length product
ACGCAAA – 5′
A
CAACAACACAAAGAACCCCCAAAAAA – 3′
ACGCAAA – 5′
A
CAACAACACAAAGAACCCCC… – 3′
CAACAACACAAAGAACCCC… – 3′
CAACAACACAAAGAACCC… – 3′
CAACAACACAAAGAACC… – 3′
CAACAACACAAAGAAC… – 3′
CAACAACACAAAGAA… – 3′
Stalled (by CTP depletion) Primed products
3′ template
3′ — UGUGUUUCUUGGGGGUUUUUU — 5′
5′ — ACACAAAGAACCCCCAAAAAA — 3′
de novo product
5′ — ACAAAAGAAA — 3′
Stalled de novo product

Supplementary Figure 10. **Misincorporation of UTP for CTP.** The effect of removing UTP from the NTP mix in the absence of CTP on the polymerase activity of purified SFTSV L protein (LP) was tested *in vitro*. The reactions were carried out with the S_{9A} 5′ RNA (nts 1-21), S_{9U} 3′ RNA (nts 1-21), and Primer B-OH present under standard polymerase assay conditions (see Materials and Methods). Products were separated by denaturing gel electrophoresis and visualised by autoradiography. Uncropped original blots/gels are provided in the Supplementary Data.

Genus/Virus	vRNA (-RNA)	cRNA (+RNA)
Mammarenaviridae		
Lassa virus (HQ688674.1)	5'– CGCACCGGGGAUCCUAGGCA –3' 3'– GCGUGGCUCCUAGGAUCCGU –5'	5'– CGCACCGAGGAUCCUAGGCA –3' 3'– GCGUGGCCCCUAGGAUCCGU –5'
Hantaviridae		
Hantaan virus (NC_005222.1)	5'– UAGUAGUAGUAUGCUCCGGA –3' 3'– AUCAUCAUCUGAGGGAUUUA –5'	5'– UAGUAGUAGACUCCCUAAAU –3' 3'– AUCAUCAUCAUACGAGGCCU –5'
Sin Nombre virus (NC_005217.1)	5'– UAGUAGUAUGCUCCGAGAAC –3' 3'– AUCAUCAUCUGAGGCUCUAU –5'	5'– UAGUAGUAGACUCCGAGAUA –3' 3'– AUCAUCAUACGAGGCUCUUG –5'
Phenuiviridae		
Severe fever with thrombo-cytopenia syndrome virus (HQ116417.1)	5'– ACACAAAGACCGCCCAGAUC –3' 3'– UGUGUCUCUGCGGGUCUACU –5'	5'– ACACAGAGACGCCCAGAUGA –3' 3'– UGUGUUUCUGGCGGGUCUAG –5'
Rift Valley fever virus (NC_014397.1)	5'– ACACAAAGACCGCCCAAUAU –3' 3'– UGUGUUUCCGCGGGUUAGUA –5'	5'– ACACAAAGGCGCCCAAUCAU –3' 3'– UGUGUUUCUGGCGGGUUAUA –5'
Nairoviridae		
Crimean-Congo hemorrhagic fever virus (NC_005301.3)	5'– UCUCAAAGAUAUAGCUAAGA –3' 3'– AGAGUUUCUAUAGUUAGGGG –5'	5'– UCUCAAAGAUAUCAAUCCCC –3' 3'– AGAGUUUCUAUAUCGAUUCU –5'
Nairobi sheep disease virus (NC_034387.1)	5'– UCUCAAAGAAAUCGUUCCCC –3' 3'– AGAGUUUCUAUAGUUAGGGG –5'	5'– UCUCAAAGAUAUCAAUCCCC –3' 3'– AGAGUUUCUUUAGCAAGGGG –5'
Peribunyaviridae		
La Crosse virus (AF528165.1)	5'– AGUAGUGUGCCCCUAUCUAC –3' 3'– UCAUCACAUGGGGAUAGAUG –5'	5'– AGUAGUGUACCCCUAUCUAC –3' 3'– UCAUCACACGGGGAUAGAUG –5'

Supplementary Figure 11. **Comparison of the 5′ and 3′ L gene ends for a selection of different bunyaviruses.** For each bunyavirus, the first 20 nts of the 5′ and 3′ ends of the genomic (-RNA) and antigenomic (+RNA) L gene are shown: nts coloured green are complementary, nts coloured black are not complementary. Sequences taken from the publicly-available RefSeq (NCBI Reference Sequence) Database.

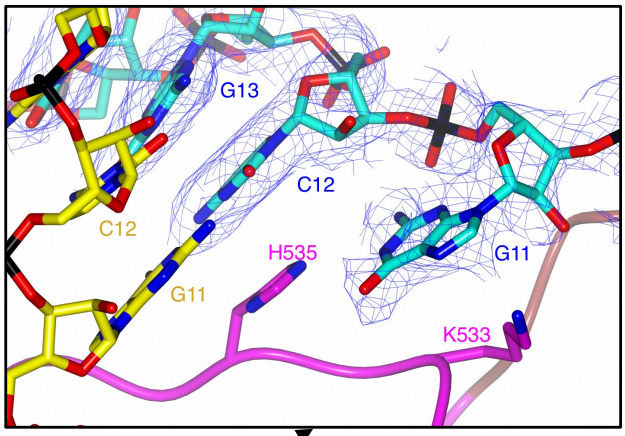

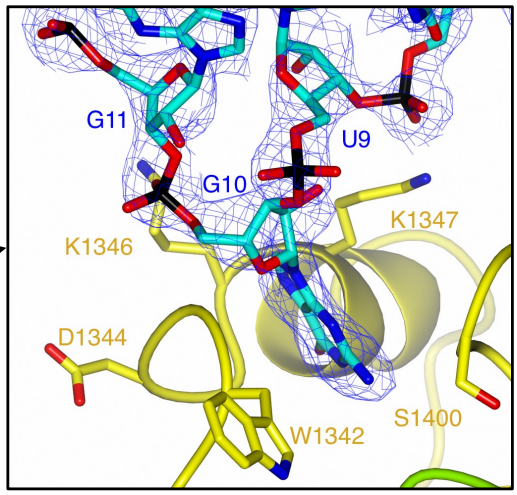

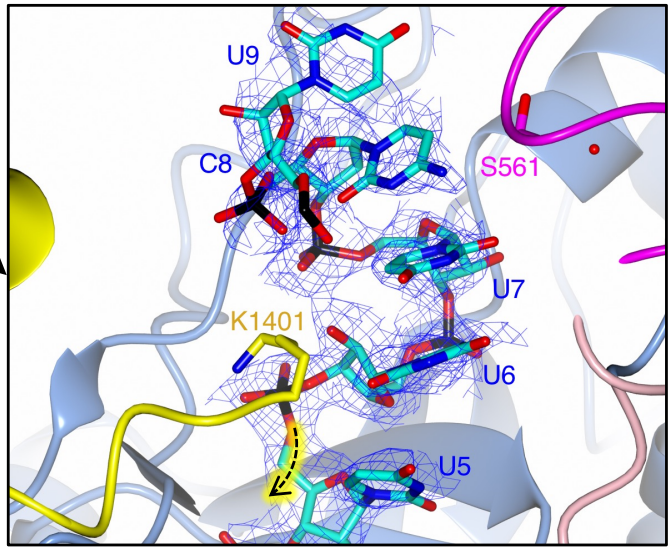

Residue 1402 onwards

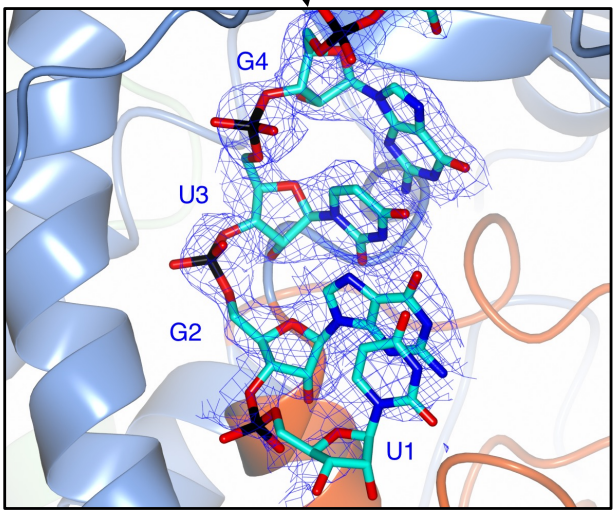

Product RNA hidden for clarity

Supplementary Figure 12. **Fitting of the 3′ RNA between the distal duplex and the template entry channel.** An overview of the EARLY-ELONGATION structure is shown as a ribbon with the protein in dark grey. The RNA in the EARLY-ELONGATION structure is shown as sticks and coloured yellow (5′ RNA) and cyan (3′ RNA). Zoomed-in views of the 3′ RNA in the space between the distal duplex and the template entry channel are shown in four panels. In each panel, the protein backbone and selected residues are coloured according to the protein domain: vRBL (magenta), thumb (green), thumb ring (yellow), PA-C like (light pink), and core lobe (blue). Key interacting residues and individual 3′ RNA nts are labelled accordingly. The map is shown and clipped to the 3′ RNA contoured at 4σ.

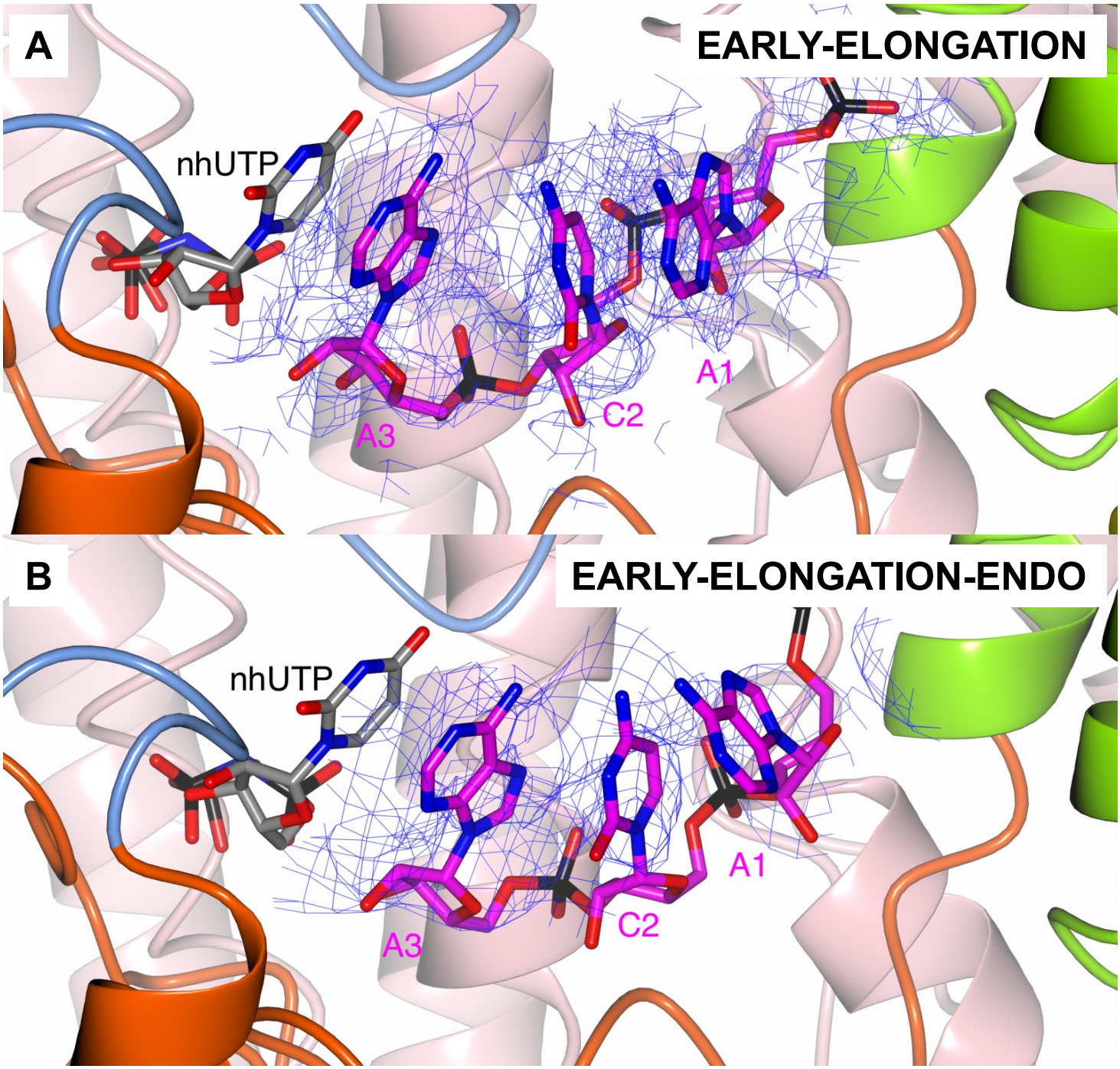
A
EARLY-ELONGATION
nhUTP
A1
C2
A3
B
EARLY-ELONGATION-ENDO
nhUTP
A1
C2
A3

Supplementary Figure 13. **State of the product RNA at early-elongation.** The product RNA is shown in the L protein core in the EARLY-ELONGATION (top) and EARLY-ELONGATION-ENDO (bottom) panels with the stalling nhUTP shown at the +1 position. For clarity, the template RNA is not shown in either panel. In both panels, the volume into which the product RNA nts have been fit is shown and is contoured at 2σ.

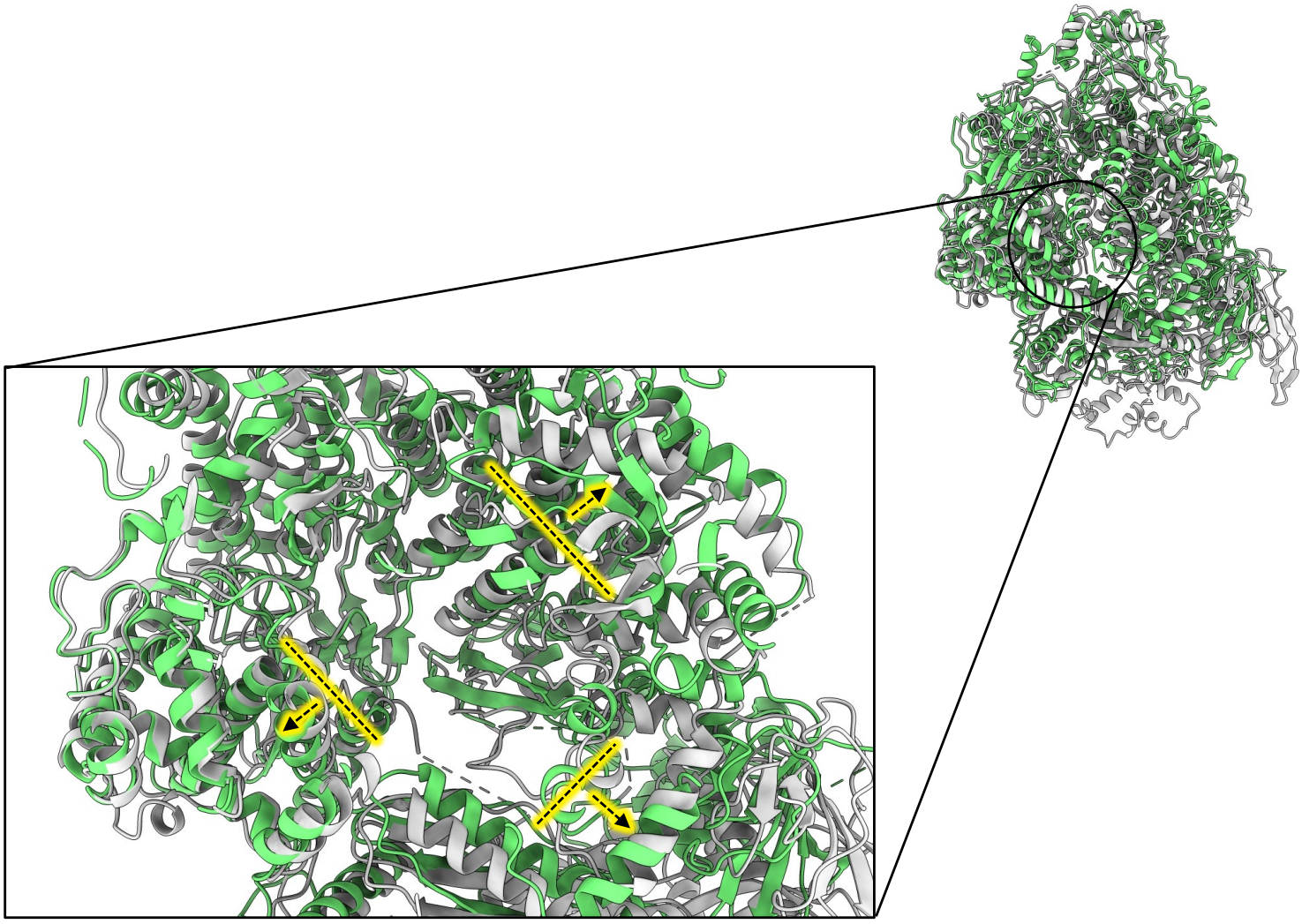

Supplementary Figure 14. **Relaxation of the L protein core from pre-initiation to late-stage elongation.** The protein backbone from the published apo structure (PDB: 7ALP) and the LATE ELONGATION structures are shown in grey and green, respectively. In the zoomed-in view, dashed lines with arrows indicate the principal direction of movement from apo to late-stage elongation. For clarity, the RNA in the L protein core in the LATE ELONGATION structure is not shown.

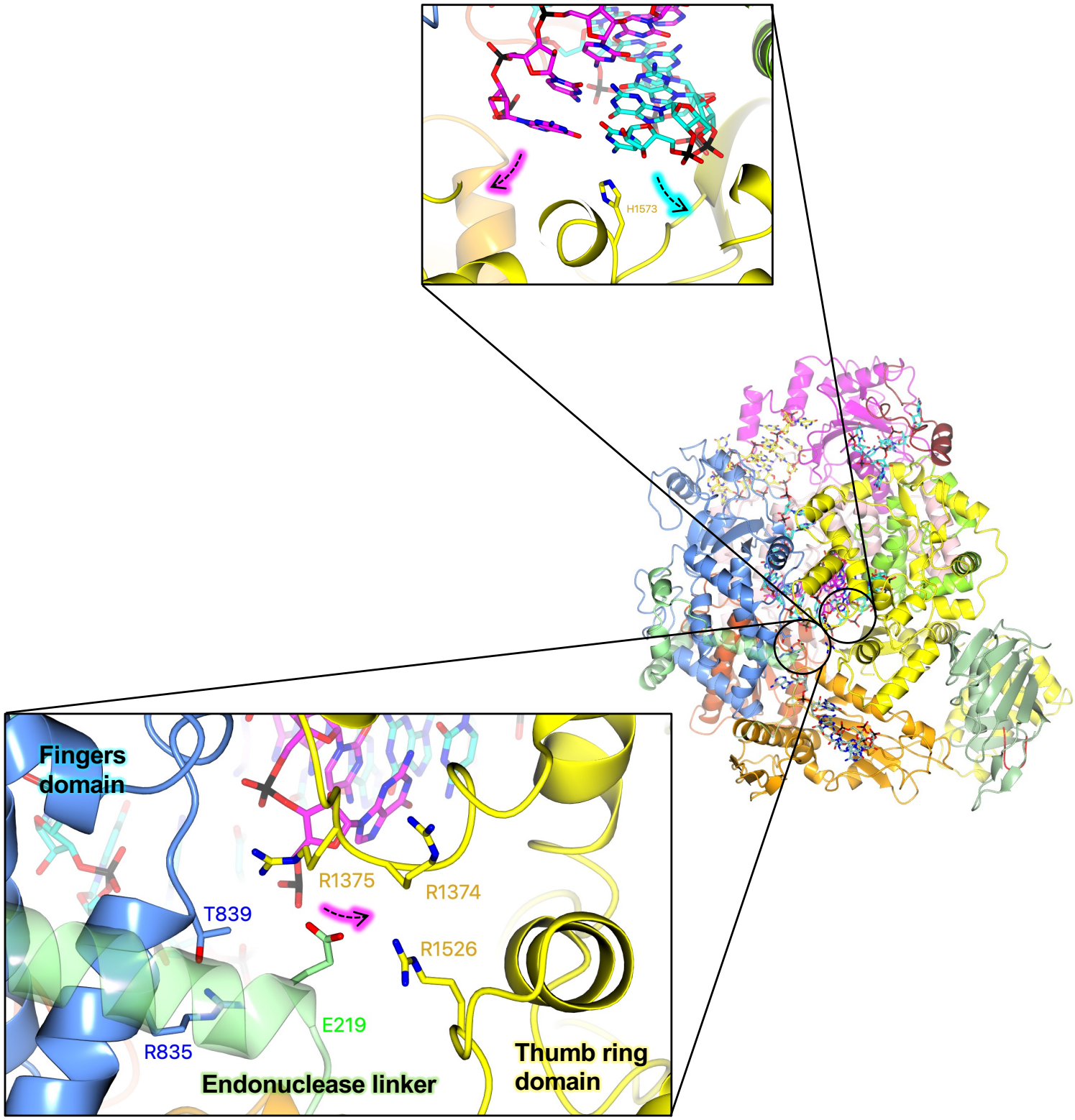
H1573
Fingers domain
R1375
R1374
T839
R1526
E219
R835
Endonuclease linker
Thumb ring domain

Supplementary Figure 15. **The putative SFTSV L protein product exit channel at late-stage elongation.** In the top zoomed-in view, the base of the product-template duplex with the H1573 sidechain buttressing the template RNA (shown in yellow) is shown. The direction of the product (shown in magenta) are indicated by dashed arrows. In the bottom zoomed-in view, the proposed exit channel in the L protein is open under apo/resting conditions and is composed of sidechains from several L protein domains, including E219 (endonuclease-linker), T839 and R835 (PA-C like domain), R1374 – R1375 and R1526 (thumb ring domain). These sidechains are shown as sticks and labelled. The path of the product RNA, which is coloured magenta, is indicated by a dashed arrow.

TOP-DOWN VIEW

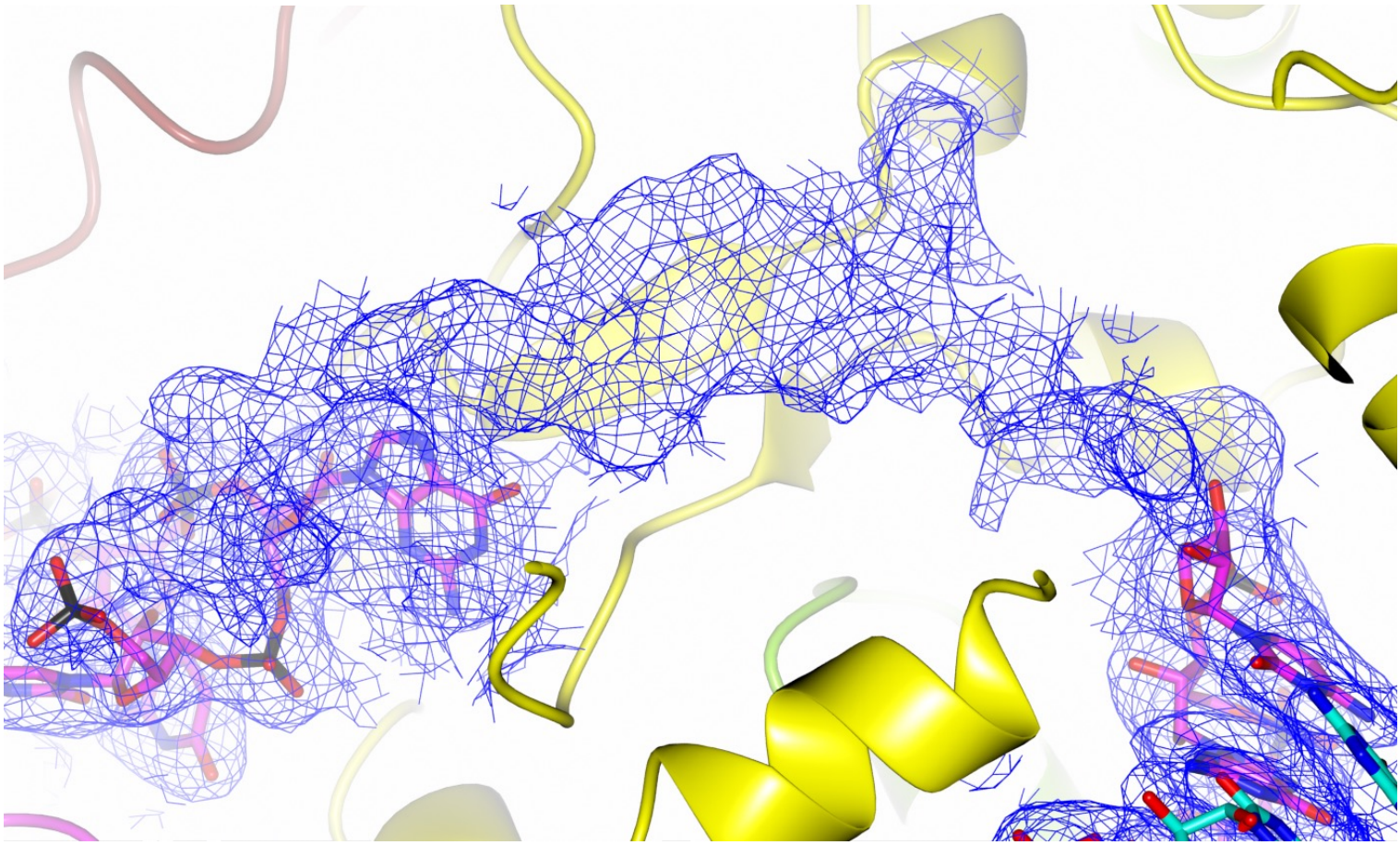

RNA in the 3’ secondary binding site

RNA in the L protein core

SIDE-ON VIEW

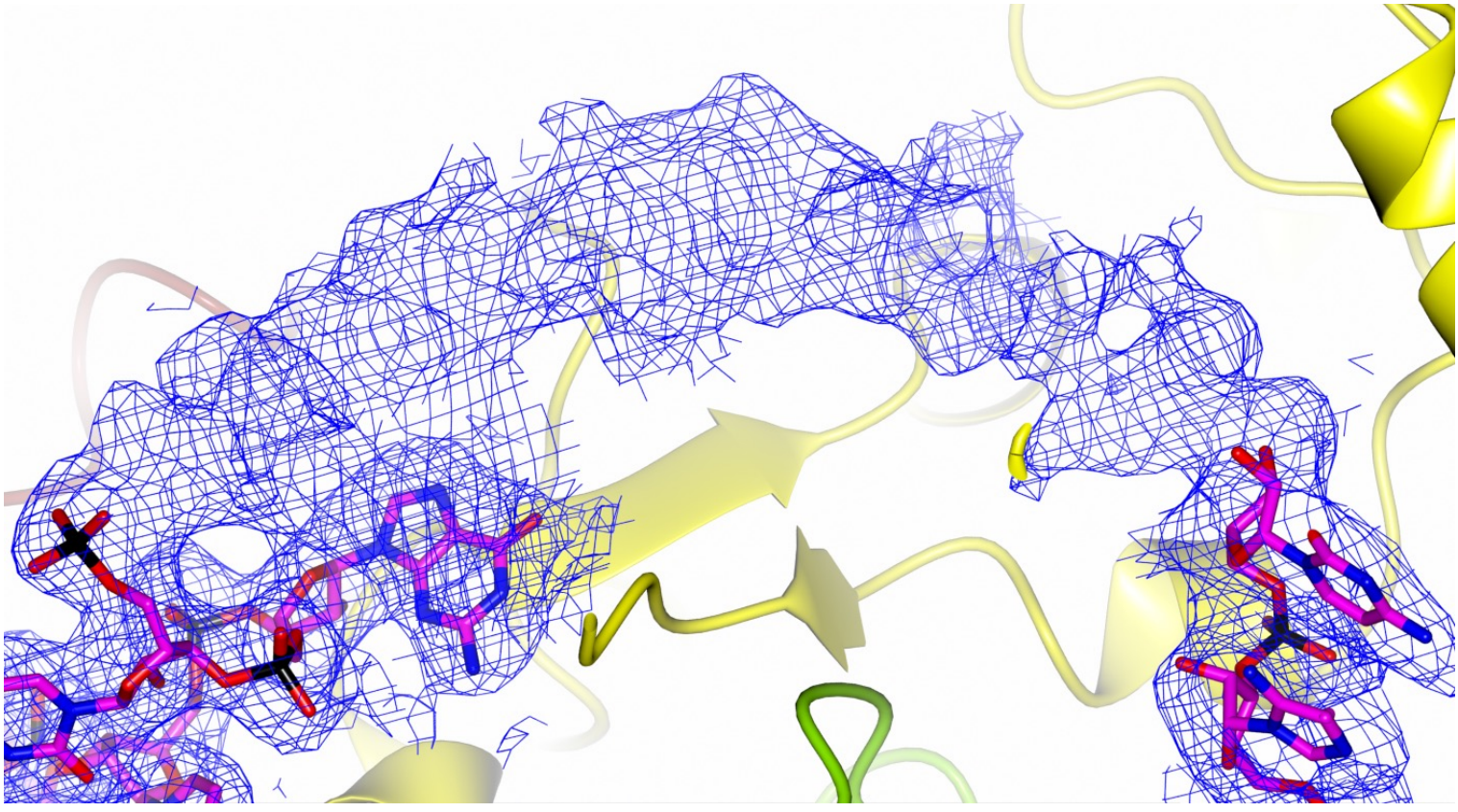

RNA in the 3’ secondary binding site

RNA in the L protein core

Supplementary Figure 16. **Blurred maps showing progression of the 3′ RNA towards the 3′ secondary binding site.** The volume in the space between the template exit channel and the 3′ secondary binding site in the LATE ELONGATION structure is shown in a top-down (top panel) and side-on (rotated by 90°) view (bottom panel). The volume was blurred by a factor of -50 in Coot and then contoured at 4σ. demonstrating that there is unbroken density between the 3′ RNA in the L protein core and the RNA fit in the 3′ secondary binding site.

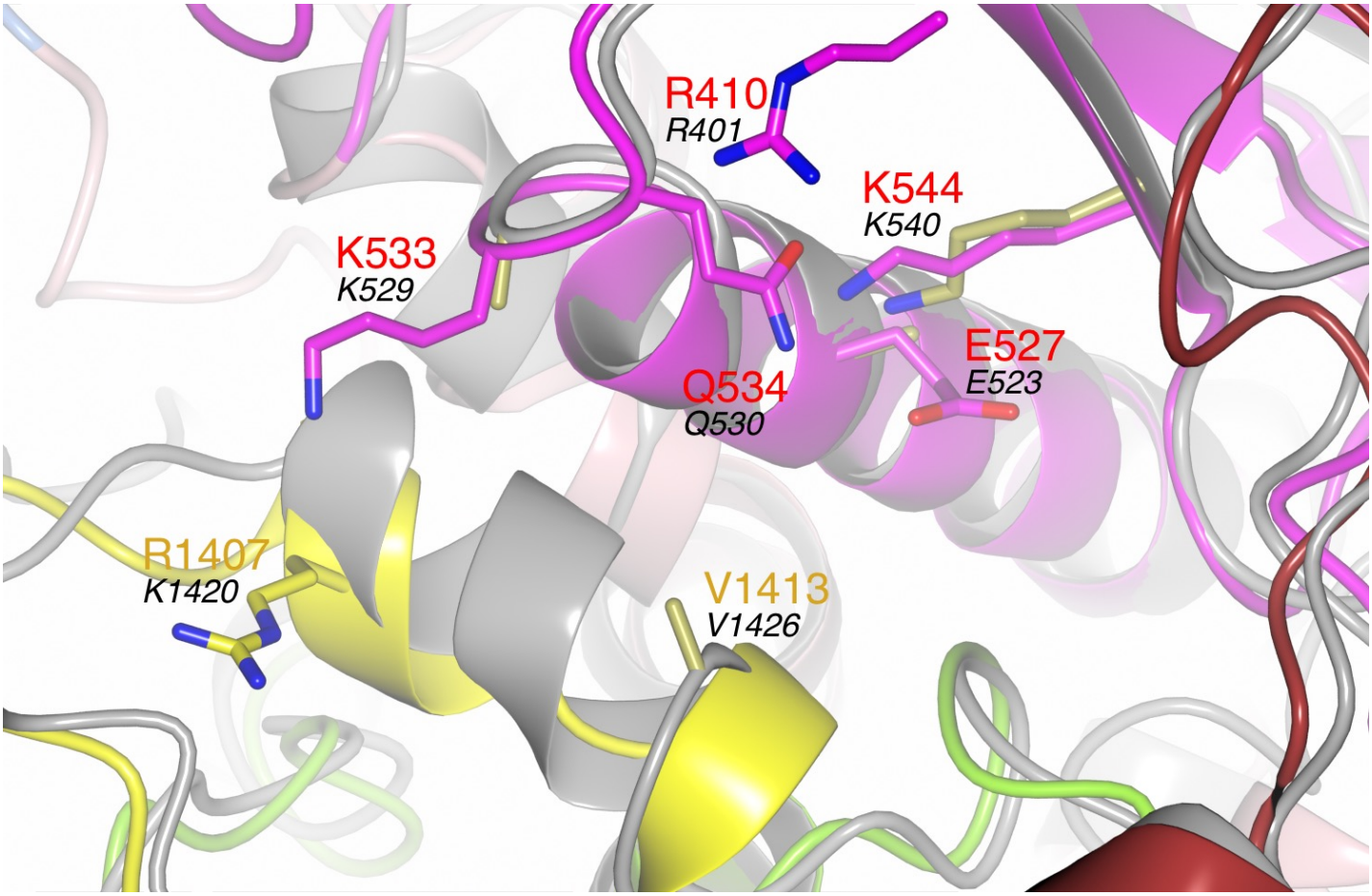


```
      370                                                  420  510    516
SFTSV LDVSLGNVEGVVSDPAKELDIAISDDPEKDTPKEAKITYRRFKPALSSSA … LSSNVVQ
 RVFV TSANLEEIERMHDDAAAELEFALSGVKDR--PD-ERNRYHRVHLNMGSDD … MGSRIGS

      517                                                          576
SFTSV WSLWVSCLAQELASALKQHCRAGEFIIKKLKFWPIYVIIKPTKSSSHIFYSLGIRKADVT
 RVFV WCQMVSLIGAELSASVKQHVKPNYFVIKRLLGSGIFLLIKPTSSKSHIFVSFAIKRSCWA

      577                          600  1406                        1436
SFTSV R-RLTGRVFSDTIDAGEWELTEFKS  …  PRVVAAGVYLLSRHCFRFSSSIHGRGSTQKA
 RVFV FDLSTSRVFKPYIDAGDLLVTDFVS  …  CKVMASAVYFLSATIFEDTGRPEFN-FLEDS
```

Supplementary Figure 17. **Structural superposition of the RVFV L protein onto the SFTSV L protein (focus on the 3′ secondary binding site).** The SFTSV L protein (LATE-ELONGATION) is shown with the RVFV L protein (PDB: 7EEI, backbone coloured grey) superposed by SSM in CCP4mg [51]. Sidechains of key amino acids mutated in the cell-based mini-replicon are shown individually. Several RVFV L protein amino acid sidechains appear truncated, this is because they were truncated in the 7ALP structure by the depositing authors. Residues from the SFTSV L protein are labelled and coloured according to the assigned domain (pink for the PA-C like-domain, magenta/red for the vRBL, green for the thumb domain, and yellow for the thumb ring) with the corresponding RVFV L protein residues shown in black text. For clarity, not all the residues mutated in the cell-based mini-replicon are shown but only 7 of the 10 in total. Created using CCP4mg. A multiple-alignment diagram showing the SFTSV (UniProtKB: F1BV96) and RVFV (UniProtKB: A2SZS3) L protein chains generated using Clustal Omega [77] is also provided. Residues mutated in the RVFV mini-replicon system are in bold with single mutants coloured red and double-mutants coloured blue.

[77] Sievers, F., Wilm, A., Dineen, D., Gibson, T.J., Karplus, K., Li, W., Lopez, R., McWilliam, H., Remmert, M., Soding, J. et al. (2011) Fast, scalable generation of high-quality protein multiple sequence alignments using Clustal Omega. Mol Syst Biol, 7, 539.

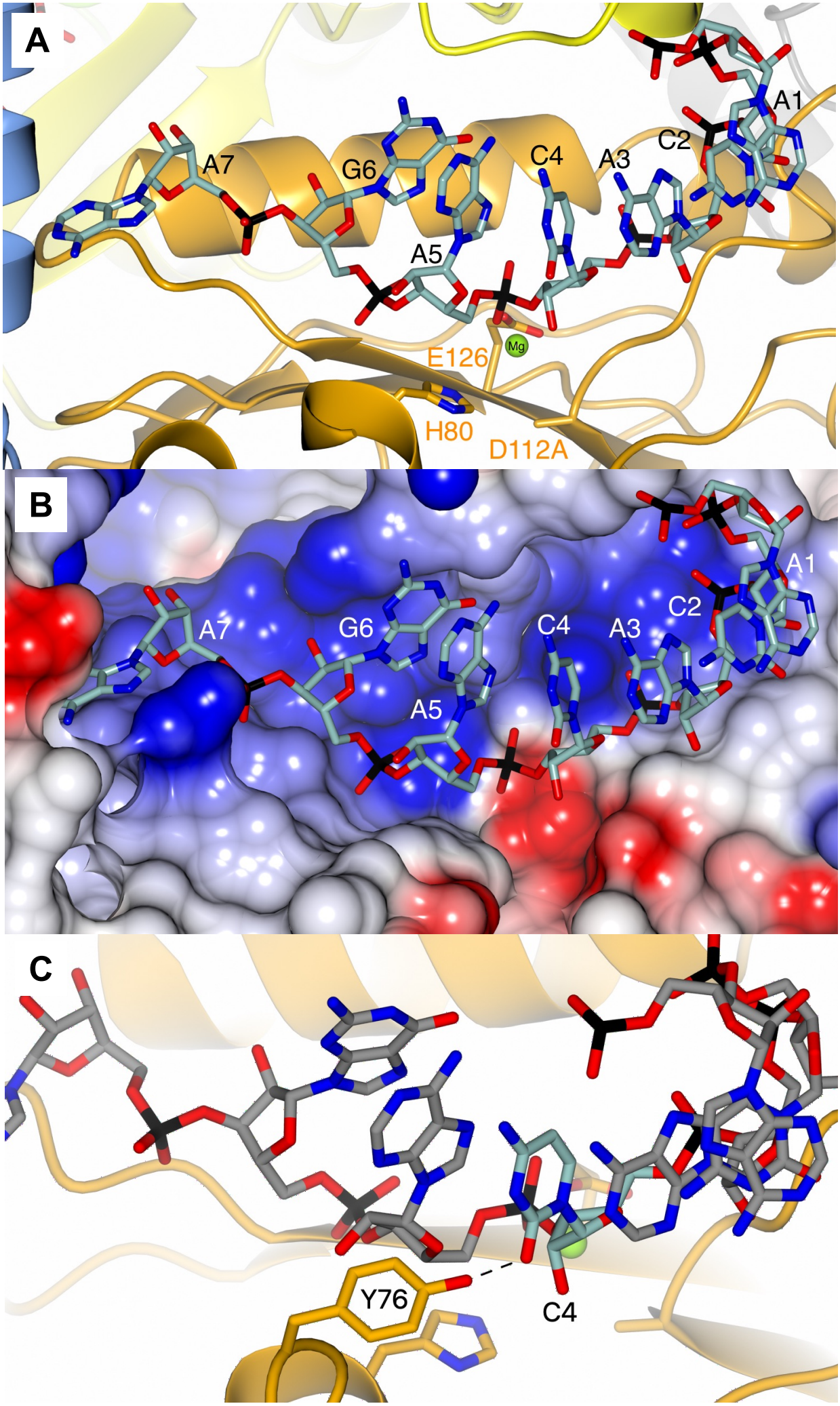
A
A7
G6
C4
A3
C2
A1
A5
Mg
E126
H80
D112A
B
A7
G6
C4
A3
C2
A1
A5
C
Y76
C4

Supplementary Figure 18. **Coordination of RNA across the SFTSV L protein endonuclease domain.** (A) The SFTSV L protein (LATE-ELONGATION) structure is shown focussed on the endonuclease domain. The L protein is coloured according to domain with the endonuclease, PA-C like-domain, and thumb/thumb ring domains coloured orange, blue, and yellow, respectively. The endonuclease-bound RNA is shown as cylinders and coloured sea green. Three of the main amino acid sidechains involved in catalysis are highlighted. These are H80, E126, and D112, the latter of which has been mutated in our experiments to an alanine, hence explaining the lack of sidechain. The endonuclease-bound RNA is labelled from the 5′ end. (B) The same view as in A but with surface electrostatics overlaid showing that the RNA is bound in a positively charged cleft across the endonuclease surface. (C) A similar, zoomed, view to that shown in A demonstrating the Y76 sidechain interacting with endonuclease-bound RNA. Here, for clarity, the endonuclease-bound RNA is coloured grey with only C4 coloured sea green.

A

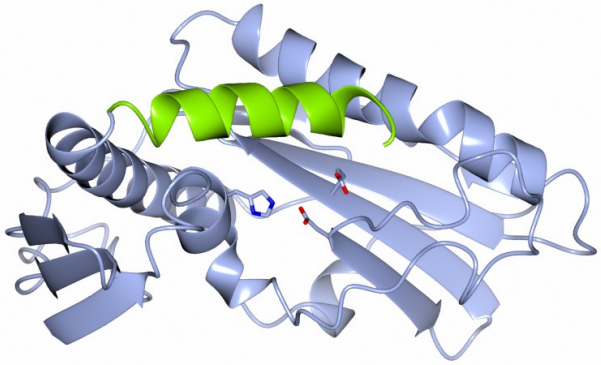

SFTSV Crystal Structure
PDB: 6NTV

B

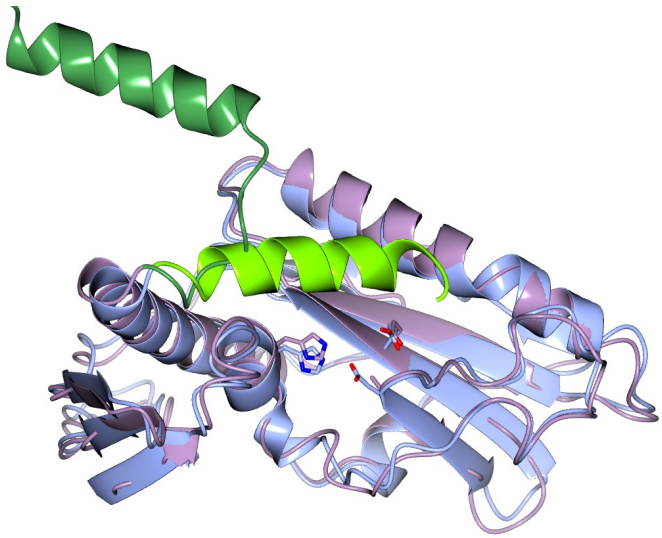

C

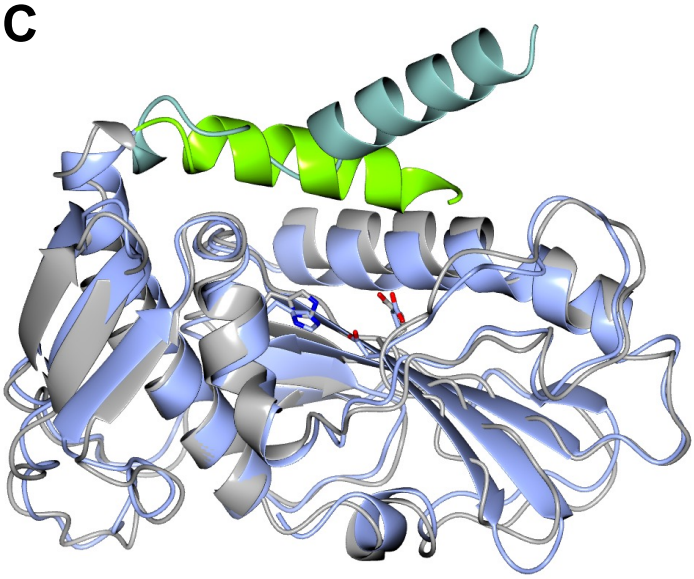

D

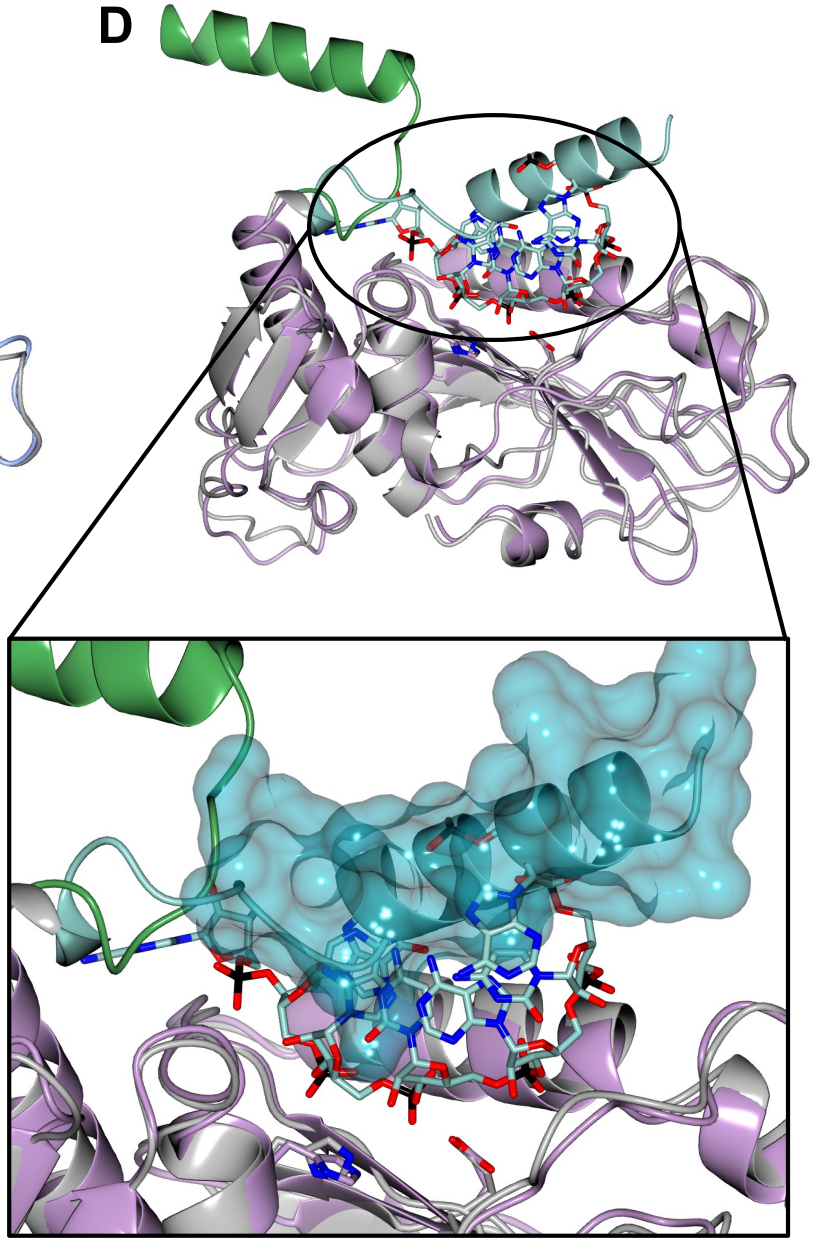

Supplementary Figure 19. **Insights into SFTSV endonuclease regulation.** (A) The published SFTSV endonuclease crystal structure, PDB: 6NTV, is shown. The protein is coloured in ice blue with α helix 6 (α6, residues 211-226) shown in light green. (B) The same view as in A but with residues 1-234 of the EARLY-ELONGATION structure superposed. The EARLY-ELONGATION structure is coloured lilac with α6 (residues 211-234) shown in dark green. (C) The same view as in A but with residues 1-234 of the EARLY-ELONGATION-ENDO structure superposed. The EARLY-ELONGATION-ENDO structure is coloured dark grey with α6 (residues 211-234) shown in sea green. (D) The EARLY-ELONGATION structure is shown as in B, however, the residues 1-234 of the EARLY-ELONGATION-ENDO have also been superposed. The EARLY-ELONGATION-ENDO structure is coloured as in C. The endonuclease-bound RNA from the LATE-ELONGATION structure is also shown and is coloured yellow. A zoomed-in view of α6 is provided with the helix surface shown. In A-D, the three putative Me^{2+} coordinating sidechains (H80, D112 in the crystal structure but D112A in our cryo-EM structures, and E126) are shown and coloured according to the protein mainchain. Structures were superposed by a least-squares fit of the indicated residue ranges in CCP4mg [51].